

# Supercontinuum generation in a photonic crystal fiber with two zero-dispersion wavelengths tapered to normal dispersion at all wavelengths

Peter Falk, Michael H. Frosz, and Ole Bang

Research Center COM, Technical University of Denmark,  
DTU Building 345V, 2800 Kongens Lyngby, Denmark

[pf@com.dtu.dk](mailto:pf@com.dtu.dk)

**Abstract:** We numerically study supercontinuum generation in photonic crystal fibers with two zero-dispersion wavelengths, weakly tapered to have normal dispersion at all wavelengths after a certain distance. We pump with 15 fs pulses with milliwatt average power and show that two distinct smooth spectral parts are generated, with improved stability due to the normal dispersion. We characterize the two spectral parts and show how the 3 dB bandwidth, the center wavelength, and the power of the two parts depend on the taper parameters and the pump power.

© 2005 Optical Society of America

**OCIS codes:** (060.4370) Nonlinear optics, fibers; (190.5530) Pulse propagation and solitons

---

## References and links

1. T.A. Birks, W.J. Wadsworth, and P.St.J. Russell, "Supercontinuum generation in tapered fibers," *Opt. Lett.* **25**, 1415-1417 (2000).
2. J.K. Ranka, R.S. Windeler, and A.J. Stentz, "Visible continuum generation in air-silica microstructure optical fibers with anomalous dispersion at 800 nm," *Opt. Lett.* **25**, 25-27 (2000).
3. S.A. Diddams, D.J. Jones, J. Ye, S. T. Cundiff, J.L. Hall, J.K. Ranka, R.S. Windeler, R. Holzwarth, T. Udem, and T.W. Hänsch, "Direct link between microwave and optical frequencies with a 300 THz femtosecond laser comb," *Phys. Rev. Lett.* **84**, 5102-5105 (2000).
4. T. Morioka, H. Takara, S. Kawanishi, O. Kamatani, K. Takiguchi, K. Uchiyama, M. Saruwatari, H. Takahashi, M. Yamada, T. Kanamori, and H. Ono, "1Tbit/s (100Gbit/s x 10 channel) OTDM/WDM transmission using a single supercontinuum WDM source," *Electron. Lett.* **32**, 906-907 (1996).
5. I. Hartl, X.D. Li, C. Chudoba, R.K. Ghanta, T.K. Ko, J.G. Fujimoto, J.K. Ranka, and P.S. Windeler, "Ultra-high-resolution optical coherence tomography using continuum generation in an air silica microstructure optical fiber," *Opt. Lett.* **26**, 608-610 (2001).
6. A. Unterhuber, B. Považay, K. Bizheva, B. Hermann, H. Sattmann, A. Stingl, T. Le, M. Seefeld, R. Menzel, M. Preusser, H. Budka, Ch. Schubert, H. Reitsamer, P.K. Ahnelt, J.E. Morgan, A. Cowey, and W. Drexler, "Advances in broad bandwidth light sources for ultrahigh resolution optical coherence tomography," *Phys. Med. Biol.* **49**, 1235-1246 (2004).
7. J.M. Dudley, L. Provino, N. Grossard, H. Maillotte, R.S. Windeler, B.J. Eggleton, and S. Coen, "Supercontinuum generation in air-silica microstructured fibers with nanosecond and femtosecond pulse pumping," *J. Opt. Soc. Am. B* **19**, 765-771 (2002).
8. S. Coen, A.H.L. Chau, R. Leonhardt, J.D. Harvey, J.C. Knight, W.J. Wadsworth, and P.St.J. Russell, "Supercontinuum generation by stimulated Raman scattering and parametric four-wave mixing in photonic crystal fibers," *J. Opt. Soc. Am. B* **19**, 753 (2002).
9. A. V. Husakou and J. Herrmann, "Supercontinuum generation, four-wave mixing, and fission of higher-order solitons in photonic-crystal fibers," *J. Opt. Soc. Am. B* **19**, 2171-2182 (2002).
10. N.I. Nikolov, T. Sørensen, O. Bang, and A. Bjarklev, "Improving efficiency of supercontinuum generation in photonic crystal fibers by direct degenerate four-wave mixing," *J. Opt. Soc. Am. B* **20**, 2329-2337 (2003).

11. N.R. Newbury, B.R. Washburn, R.S. Windeler, and K.L. Corwin, "Noise amplification during supercontinuum generation in microstructure fiber," *Opt. Lett.* **28**, 944-946 (2003).
12. K.L. Corwin, N.R. Newbury, J.M. Dudley, S. Coen, S.A. Diddams, K. Weber, and R.S. Windeler, "Fundamental noise limitations to supercontinuum generation in microstructure fiber," *Phys. Rev. Lett.* **90**, 113904 (2003).
13. C.M. Netti, M.E. Zoorob, S. Roberts, M.D. Charlton, G.J. Parker, J.J. Baumberg, J.R. Lincoln, M.J. Lederer, and D. Kopf, "Low noise self-phase modulation continuum generation in high index tapered planar waveguide at 1040nm for OCT applications," paper 5690-38, Photonic West, San Jose, USA, Jan. 22-27, 2005.
14. K.M. Hilligsøe, T.V. Andersen, H.N. Paulsen, C.K. Nielsen, S.R. Keiding, S. Kristiansen, K.P. Hansen, and J.J. Larsen, "Supercontinuum generation in a photonic crystal fiber with two zero dispersion wavelengths," *Opt. Express* **6**, 1045-1054 (2004). <http://www.opticsexpress.org/abstract.cfm?URI=OPEX-12-6-1045>
15. M.H. Frosz, P. Falk, and O. Bang, "The role of the second zero-dispersion wavelength in generation of supercontinua and bright-bright soliton-pairs across the zero-dispersion wavelength," *Opt. Express* **13**, 6181-6192 (2005). <http://www.opticsexpress.org/abstract.cfm?URI=OPEX-13-16-6181>
16. J.M. Schmitt, S.H. Xiang, and K.M. Yung, "Differential absorption imaging with optical coherence tomography," *J. Opt. Soc. Am. A* **15**, 2288-2296 (1998).
17. F. Lu, Y. Deng, and W.H. Knox, "Generation of broadband femtosecond visible pulses in dispersion-managed holey fibers," *Opt. Lett.* **30**, 1566-1568 (2005).
18. S.G. Johnson and J.D. Joannopoulos, "Block-iterative frequency-domain methods for Maxwell's equations in a planewave basis," *Opt. Express* **8**, 173-190 (2001). <http://www.opticsexpress.org/abstract.cfm?URI=OPEX-8-3-173>
19. G.P. Agrawal, *Nonlinear Fiber Optics*, 2nd edition (Academic, New York, 2001).

## 1. Introduction

Supercontinuum generation (SCG) in optical fibers has been studied for more than two decades. In 2000 it was shown that SCG can be made particularly efficient in tapered fibers [1] and photonic crystal fibers (PCFs) [2], due to the increased effective nonlinearity and the large degree of freedom in tailoring the dispersion profile. The first supercontinuum (SC) light sources are now commercially available and find important applications in areas such as frequency metrology [3], wavelength division multiplexing [4], and optical coherence tomography (OCT) [5].

Here, our focus is on PCF-based SCG broadband light sources for application in OCT. In this context fiber based light sources are attractive due to their diversity with respect to center wavelength, bandwidth and output power. For an excellent review of the advances in broad bandwidth light sources for OCT we refer to Unterhuber *et al.* [6]. In OCT the axial resolution scales with the center wavelength squared and the inverse of the 3 dB bandwidth. PCF-based SCG light sources with octave-spanning bandwidths have consequently received considerable interest [6]. However, for OCT applications the spectrum should be smooth and Gaussian, or at least close-to-Gaussian over the 3 dB bandwidth, in order to avoid multiple image echoes that may hide weak object structures and reduce image resolution and sensitivity.

Typical ultra-broad SC spectra in PCFs are generated through an interplay between several nonlinear effects in the anomalous dispersion regime [7, 8, 9, 10]. This results in significant power fluctuations, spectral modulations, and excess noise [11, 12]. Consequently such SC spectra have to be filtered to obtain a near-Gaussian shape, which results in a considerable loss of power. One way to avoid these spectral fluctuations is to pump in the normal dispersion regime far from the zero-dispersion wavelength. This eliminates modulational instability (MI) and soliton effects, such as soliton fission and soliton self-frequency shift (SSFS), and means that only self-phase modulation (SPM) will be present. This leads to improved stability properties and a shape that is closer to a Gaussian, but also to a reduced spectral broadening [13].

In a recent interesting study, SCG in a PCF with two closely spaced zero-dispersion wavelengths (ZDWs) at 780 nm and 945 nm was investigated both experimentally and numerically. It was shown that two smooth spectral parts were generated, which were described as being stable and compressible, with a high spectral density only weakly dependent on pump parameters over a wide range of pulse parameters [14]. It was argued that the generated SC was a result

of initial SPM followed by FWM, whereas we have recently shown that it is in fact SPM and generation of dispersive waves, followed by SSFS if the separation between the ZDWs is large enough, that are at play [15].

The smooth two-part spectrum observed in [14] could in fact be an attractive light source for OCT, due to the near Gaussian shape of the two spectral parts. The spectral part with the lowest power content could be filtered away or both parts could be used in a differential absorption OCT scheme with improved spectroscopic information [16].

On a different note it was recently demonstrated how a PCF can be tapered to modulate its dispersion properties for desired applications [17]. Of course the dispersion profile of a PCF can be designed from the start at the fabrication stage, but tapering is a post manufacturing technique that provides an attractive way of manipulating the dispersion and, in a cheap and relatively easy way, obtain PCFs with different properties without drawing a new PCF.

Here we combine the advantageous properties of normal dispersion, tapering, and the PCF with two ZDWs. Specifically we use the tapering to 1) gradually move the ZDWs and thereby the center wavelength of the two spectral parts; 2) increase the stability of the SC by tapering down to a diameter for which the dispersion is normal at all wavelengths, thereby eliminating MI and soliton effects. Because the two ZDWs are close from the start we only need to taper very weakly in order to obtain normal dispersion at all wavelengths. As a first investigation of such a light source we present a theoretical investigation of the properties of the generated two spectral parts. We show how the 3 dB bandwidth, the center wavelength, and the power of the spectral parts depend on the degree of tapering, the taper length, and the pump power.

## 2. Tapered PCF model

We consider a highly nonlinear triangular PCF with pitch  $\Lambda = \Lambda_0 = 1.0 \mu\text{m}$ , hole diameter  $d = 0.57 \mu\text{m}$ , and core diameter  $1.4 \mu\text{m}$ . We taper the PCF as shown in Fig. 1(a), assuming that the relative hole size,  $d/\Lambda$ , is constant, while the pitch,  $\Lambda(z)$ , varies as

$$\Lambda(z) = \Lambda_T \left( 1 + \frac{\Lambda_0^2 - \Lambda_T^2}{\Lambda_T^2} \frac{(z - z_T)^2}{z_T^2} \right)^{1/2}. \quad (1)$$

We define the taper as the region of the PCF in which the diameter decreases from its maximum to its minimum value. Here  $z_T$  is the length of the taper and  $\Lambda_T$  is the final pitch at the end of the taper. It was recently demonstrated that it is indeed possible to taper a PCF in this way and observe SCG [17]. We calculate the dispersion and effective area using the MIT Photonics Bands package [18]. Fig. 1(b) shows the dispersion profiles along the taper. The distance between the ZDWs narrows along the taper, i.e. for decreasing pitch, until the fiber has normal dispersion for all wavelengths for  $\Lambda < 0.96 \mu\text{m}$ . The effective area increases with wavelength from  $A_{\text{eff}} = 1 \mu\text{m}^2$  at 400 nm to  $A_{\text{eff}} = 2 \mu\text{m}^2$  at 1500 nm for  $\Lambda = 1.0 \mu\text{m}$ . The variation of  $A_{\text{eff}}$  along the taper is modest and we neglect it.

We simulate pulse propagation using the split-step Fourier method to solve the generalized nonlinear Schrödinger equation [19]. The dispersion parameters  $\beta_{2-15}$  are extracted from fits to 11 dispersion profiles with  $\Lambda$  varying from  $1.0 \mu\text{m}$  to  $0.9 \mu\text{m}$ . We then fit the  $\Lambda$ -variation of each  $\beta$ -parameter [see Fig. 1(c)] with a 2nd order polynomial to obtain an analytical formula for  $\beta_{2-15}(\Lambda)$ . In our simulations we use 100 values of the pitch in the taper from  $z = 0$  to  $z = z_T$ . The wavelength dependence of the effective area is incorporated through the nonlinear parameter  $\gamma$ . A wavelength independent loss of 50 dB/km is also included. The model accounts for SPM, FWM, stimulated Raman Scattering (SRS), and self-steepening. We simplify the investigation by assuming a polarization maintaining fiber pumped along one polarization axis. To focus on the SCG effects in the taper region of the PCF we consider a pulse launched at  $z = 0$  [see Fig. 1(a)]. The simulation is stopped at  $z = z_T$ . We pump at 808 nm with a pulse width of 15

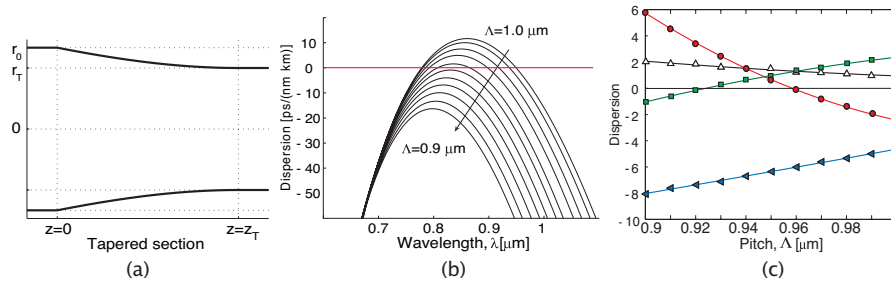


Fig. 1. (a) Dimensions and (b) dispersion profiles for the tapered triangular PCF with relative hole diameter  $d/\Lambda = 0.57$  and pitch  $\Lambda = \Lambda_0 = 1.0 \mu\text{m}$  (untapered) to  $\Lambda = \Lambda_T = 0.9 \mu\text{m}$ , in steps of  $0.01 \mu\text{m}$ . The dispersion is normal for all wavelengths for  $\Lambda < 0.96 \mu\text{m}$ . (c) Dispersion coefficients  $\beta_2 [10^{-27} \text{ s}^2/\text{m}]$  (red,  $\circ$ ),  $\beta_3 [10^{-41} \text{ s}^3/\text{m}]$  (green,  $\square$ ),  $\beta_4 [10^{-55} \text{ s}^4/\text{m}]$  (black,  $\triangle$ ), and  $\beta_5 [10^{-70} \text{ s}^5/\text{m}]$  (blue,  $\nabla$ ), versus pitch  $\Lambda$ .

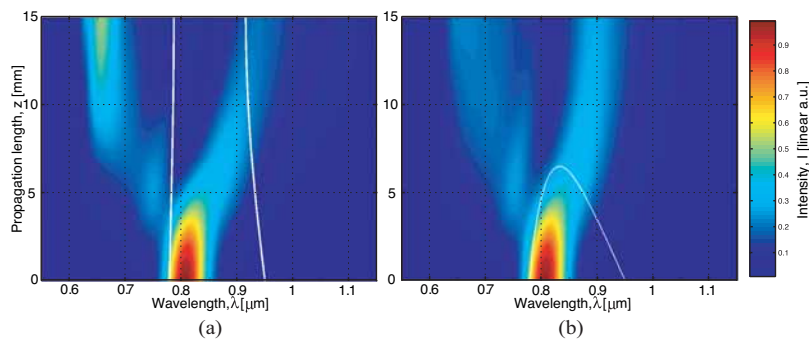


Fig. 2. Color coded power spectrum plot of the spectral evolution in a  $z_T = 15 \text{ mm}$  long taper with final pitch (a)  $\Lambda_T = 0.98 \mu\text{m}$  and (b)  $\Lambda_T = 0.93 \mu\text{m}$ . The white line represents the ZDWs with the dispersion being anomalous inside this curve.

fs, intensity FWHM. The repetition rate is 75 MHz. The peak power is 5 kW, unless otherwise noted, corresponding to an average power of 6 mW and a pulse energy of 80 pJ. This is easily achieved with commercially available Ti:Sapphire lasers. Average power is used here for the importance in exposure considerations of biological tissue.

### 3. Supercontinuum generation and spectral properties

In Fig. 2 we show how the SC spectrum evolves during propagation in a 15 mm long taper for two different values of the degree of tapering  $\Lambda_T$ . For weak tapering,  $\Lambda_T > 0.96 \mu\text{m}$  [Fig. 2(a)], SPM broadens the spectrum of the pump into the near infrared regime (NIR) and phase-matched dispersive waves are generated in the normal dispersion regime on the visual wavelength (VIS) side, as detailed in [15].

For strong tapering [Fig. 2(b)] the dispersion becomes normal at all wavelengths after 7 mm of propagation. The normal dispersion eliminates soliton effects, which stabilizes the spectrum in the sense that spectral variations with fiber length are reduced, as compared to the case without tapering. Thus tapering allows to control the center wavelength of the two spectral parts and relaxes the requirement for accurate cutting of the fiber at a specific length, because the spectrum is more fixed during propagation in the normal dispersion regime. Because MI is absent in the normal dispersion regime, we know that the spectrum will also be more stable towards intensity and phase fluctuations of the pump [13, 19].

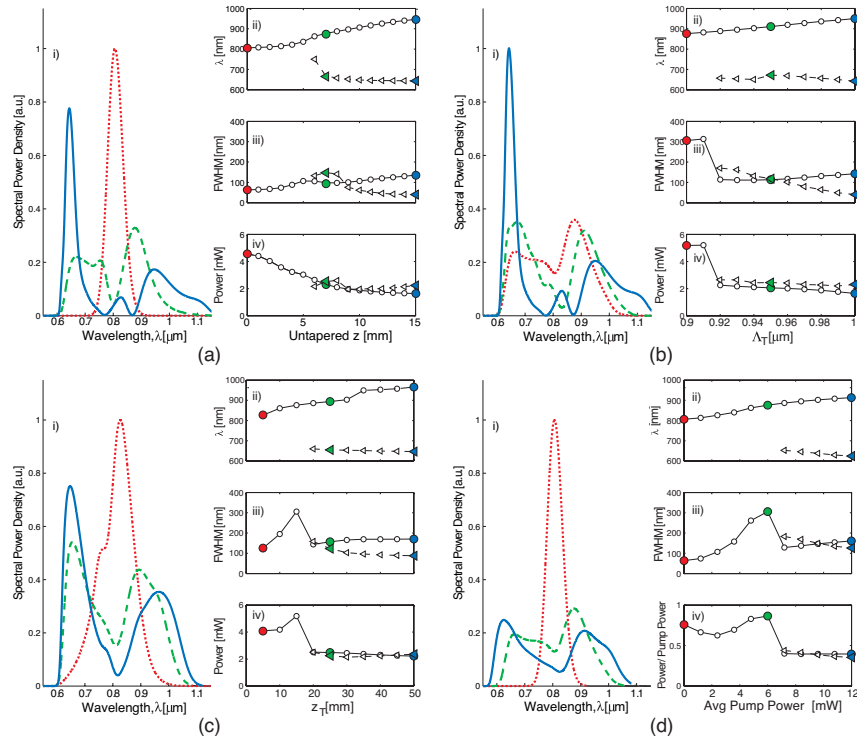


Fig. 3. (a, i) Power spectrum for an untapered PCF with  $\Lambda_T = 1.0 \mu\text{m}$  at  $z = 0 \text{ mm}$  (dotted, red),  $8 \text{ mm}$  (dashed, green), and  $15 \text{ mm}$  (solid, blue). (b, i) Power spectrum at taper end  $z = z_T = 15 \text{ mm}$  for  $\Lambda_T = 0.9 \mu\text{m}$  (dotted, red),  $0.95 \mu\text{m}$  (dashed, green), and  $1.0 \mu\text{m}$  (solid, blue). (c, i) Power spectrum for  $\Lambda_T = 0.9 \mu\text{m}$  at taper end  $z = z_T = 15 \text{ mm}$  (dotted, red),  $25 \text{ mm}$  (dashed, green), and  $50 \text{ mm}$  (solid, blue). (d, i) Power spectrum at taper end  $z = z_T = 15 \text{ mm}$  for  $\Lambda_T = 0.9 \mu\text{m}$  and average pump power  $6 \mu\text{W}$  (dotted, red),  $6 \text{ mW}$  (dashed, green), and  $12 \text{ mW}$  (solid, blue). (a-d, ii) center wavelength, (a-d, iii) FWHM, and (a-d, iv) average power within the FWHM versus respective parameters, NIR ( $\circ$ ) and VIS spectral parts ( $\triangleleft$ ).

The smooth two-part spectral structure is interesting for applications as light sources in, e.g., OCT systems. In order to investigate the spectral properties and how they depend on the taper parameters and the pump power, we have performed a comprehensive series of numerical simulations. In each case we have determined whether the spectrum has a single-peak or two-peak structure, where a peak is defined as an isolated spectral part that has its own well-defined full width at half maximum (FWHM). For each peak we have then recorded the center wavelengths, FWHM, and average power within the FWHM. The subfigures (ii), (iii), and (iv) in Fig. 3(a-d) show how these parameters vary.

In Fig. 3(a) we look at the spectral evolution during propagation in an untapered PCF, i.e., with  $\Lambda_T = \Lambda_0 = 1.0 \mu\text{m}$ . We see that after  $7 \text{ mm}$  of propagation the spectrum is split into two separate peaks. The center wavelength and FWHM of the VIS peak stabilizes after  $10 \text{ mm}$  of propagation, while the NIR peak continues to red-shift due to SSFS. The average power in the two peaks settles at around  $2 \text{ mW}$ .

In Fig 3(b) we fix the length of the fiber to  $15 \text{ mm}$  and vary the pitch at the end of the taper,  $\Lambda_T$ , from  $0.9 \mu\text{m}$  (long propagation length in the all-normal dispersion regime) to  $1.0 \mu\text{m}$ , where the fiber is untapered. The center wavelength of the NIR peak has an almost linear dependence

with  $\Lambda_T$ . Thus tapering allows to move the NIR peak while the VIS peak is fixed, both peaks with a power around 2 mW. The variation in the dispersion profile due to the tapering makes the phase matching of dispersive waves work for a broader VIS range, resulting in an increased FWHM of the VIS part. For a strong tapering,  $\Lambda_T \leq 0.91 \mu\text{m}$ , the dispersion changes so fast that the two spectral parts do not have time to separate. Thus, if a two-peak structure is desired, one cannot taper this particular PCF, with this length, too strongly.

In Fig. 3(c) we now consider a fixed strong degree of tapering,  $\Lambda_T = 0.9 \mu\text{m}$  while varying the length of the taper from  $z_T = 5 \text{ mm}$  to 50 mm. Again we see that a certain propagation length in the anomalous dispersion regime is needed to split the spectrum, with the two-peak structure first appearing for  $z_T > 20 \text{ mm}$ . The most important effect is the increased power levels and FWHM of both spectral parts, which can be achieved with a long and strong tapering.

It is important to stress, that the spectral splitting is a nonlinear process, initiated by SPM and a red-shift of the pump. Considering a tapered PCF with  $z_T = 15 \text{ mm}$  and  $\Lambda_T = 0.9 \text{ mm}$ , we observe the following: for low pump powers (average power below 7 mW) the red-shift is not strong enough to obtain splitting, as clearly seen in Fig. 3(d). For average pump powers above 7 mW splitting is observed with almost equal power in the two parts. In contrast to the observed variation of the VIS part with the other control parameters, we see that increasing the pump power allows to move the VIS part further into the blue.

#### 4. Conclusion

We have numerically investigated femtosecond SCG in a weakly tapered PCF with two closely spaced ZDWs, where the dispersion becomes normal for all wavelengths after a certain distance, provided the tapering is strong enough.

We have shown that above a certain pump power (7 mW for a 10% tapering over a length of 15 mm) the red-shift of the pump is strong and leads to a splitting of the spectrum into a blue and a red part. The initial red-shift is thus a nonlinear process due to SPM, followed by SSFS, which requires a sufficient power level. We have shown that the splitting further requires a certain propagation length in the anomalous dispersion regime, where soliton effects are present.

We have also shown how the normal dispersion spectrally stabilizes the resulting SC spectrum, in the sense that it stops the red-shift due to soliton effects and thereby tends to fix the wavelength of the two spectral parts. Because we know that MI is not present in the normal dispersion regime it is to be anticipated that the resulting spectrum is also more stable towards fluctuations of the pump, as was shown recently for SCG in a planar waveguide [13].

An important point of our study has been to investigate how tapering can be used to control the power, FWHM, and center wavelength of the two spectral parts. Our results show how the weak tapering allows to manipulate both the center wavelength and width of the two parts by up to 150 nm while the average power content remains nearly constant (about 2 mW for 6 mW average pump power). The combination of pulse propagation length and degree of tapering can result in more Gaussian shaped spectra and higher bandwidth. The spectra still broadens during propagation in the all-normal dispersion regime, limiting the required length with anomalous dispersion and nonlinear effects contributing to noise and instability.

#### Acknowledgment

P. Falk acknowledges support from The Danish Research Council for Technology and Production Sciences (FTP) under grant no. 26-02-0020.